AIAA JOURNAL
Vol. 34, No. 5, May 1996

Evaluation of the Dynamic Model for Simulations of Compressible Decaying Isotropic Turbulence

Evangelos T. Spyropoulos* and Gregory A. Blaisdell†
Purdue University, West Lafayette, Indiana 47907

Several issues involving the use of the dynamic subgrid-scale model in large-eddy simulations of compressible turbulent flows are investigated. The model is employed in simulations of compressible decaying isotropic turbulence, and its performance is compared against results from direct numerical simulations and experiments. Results from a parametric study suggest the model captures compressibility effects well. Use of the dynamic model in simulations of inhomogeneous flows requires filtering of the flowfield in physical space rather than Fourier wave space. The use of spatial filters is examined by conducting simulations of isotropic turbulence. Several implicit filters are found to perform extremely well and similar to the sharp cutoff filter. One explicit filter performed well, but all others provided excessive dissipation at higher modes. Two formulations of the dynamic model, proposed by Moin et al. and Lilly, perform well, with Lilly's being more accurate. Results suggest also a great insensitivity of the model on the filter width ratio. A modification of the convective terms in the momentum and energy equations is found to reduce the effects of aliasing errors. Finally, different formulations of the energy equation are examined. A nonconservative form is found to be more accurate.

I. Introduction

In the past few years there has been a resurgence of interest in performing large-eddy simulations (LES) of flows of engineering interest. There are two roles for LES to play in the computation of such flows. First, LES can be used to test lower order models: k–ϵ, algebraic stress, and full Reynolds stress models. LES can provide detailed data, which is difficult or impossible to measure experimentally and which is at much higher Reynolds numbers than can be reached by direct numerical simulation (DNS). Statistical data and physical insight gained from these simulations can be used to evaluate and improve the lower order models. With this approach, however, the subgrid-scale (SGS) model used in the LES has to be validated in order to ensure that the LES data are correct.

Second, LES can be used as an engineering tool rather than as a research tool. With the expected increases in computer capabilities in the near future, especially from the use of massively parallel computers, it may be feasible to perform LES of flows of engineering interest. LES will remain an expensive tool, but it will likely be the only means of accurately computing complex flows for which lower order turbulence models fail.

Recently, there has been much interest in using the dynamic SGS model to perform LES. The dynamic model was first introduced by Germano et al.[1] and was extented for use in compressible flows by Moin et al.[2] Since then, further refinements to the model have been proposed.[3–6] The main advantage of the dynamic model over other SGS models used in the past is that it requires little prior experience with the type of flow being considered. The model (dynamically) adjusts to the flow conditions by employing the resolved large-scale information to predict the effects of the small scales.

So far, the dynamic model has been mostly tested in incompressible turbulent flows and has been found to perform well. Moin et al.[2] applied the dynamic model to compressible decaying isotropic turbulence and found that it performed well and better than using fixed values for the model constants. El Hady et al.[7] applied the model to a transitional supersonic axisymmetric boundary layer with satisfactory results. However, a number of issues regarding the use of the model in LES of compressible turbulence remain to be addressed, such as the ability of the model to capture compressibility effects without the need for explicit compressibility corrections.

In addition, there are issues that need to be addressed in applying the dynamic model to inhomogeneous flows. The dynamic model requires filtering the resolved large-scale field. So far, it has been mostly implemented in turbulent flows that are homogeneous in at least two directions where the filtering can be performed efficiently (and exactly) in wave space using fast Fourier transforms. In more complex inhomogeneous flows, this is not possible, and some kind of discrete filtering has to be applied in physical space. In simulations of such flows, three-point explicit filters have been mostly used. A number of other spatial filters are available and require testing.

The main objective of this paper is to examine the performance of the dynamic SGS model in the context of compressible decaying isotropic turbulence. The model is evaluated by making comparisons with results from direct numerical simulations, as well as with reported "high" Reynolds number, nearly incompressible experimental data. The simulations are used to assess the capture of compressibility effects and to investigate issues regarding the implementation of the dynamic model for inhomogeneous flows. The reason for considering homogeneous turbulence is that the performance of the dynamic model can be evaluated separately from the effects of inhomogeneity.

II. Mathematical Formulation

A. Governing Equations

In LES one computes the motion of the large-scale structures, while modeling the nonlinear interactions with the small scales. The governing equations for the large eddies in compressible flows are obtained after filtering the continuity, momentum, and energy equations and recasting in terms of Favre averages. The filtering operation (denoted by an overbar) maintains only the large scales and can be written in terms of a convolution integral,

$$\bar{f}(\boldsymbol{x}) = \int_D G(\boldsymbol{x} - \boldsymbol{x}') f(\boldsymbol{x}')\, \mathrm{d}\boldsymbol{x}' \tag{1}$$

where f is a turbulent field, G is some spatial filter (usually a sharp cutoff defined in Fourier space) of width equal to the grid spacing, and D is the flow domain.

Received Jan. 5, 1995; presented as Paper 95-0355 at the AIAA 33rd Aerospace Sciences Meeting, Reno, NV, Jan. 11–14, 1995; revision received May 19, 1995; accepted for publication May 22, 1995.

*Graduate Assistant, School of Aeronautics and Astronautics. Member AIAA.
†Assistant Professor, School of Aeronautics and Astronautics. Member AIAA.

The resulting equations of motion are as follows:

$$\frac{\partial \bar{\rho}}{\partial t} + \frac{\partial}{\partial x_i}(\bar{\rho}\tilde{u}_i) = 0 \tag{2}$$

$$\frac{\partial}{\partial t}(\bar{\rho}\tilde{u}_i) + \frac{\partial}{\partial x_j}(\bar{\rho}\tilde{u}_i\tilde{u}_j) = \frac{\partial}{\partial x_j}(\tilde{\sigma}_{ij}) - \frac{\partial}{\partial x_j}(\tau_{ij}) \tag{3}$$

$$C_v\frac{\partial}{\partial t}(\bar{\rho}\tilde{T}) + C_v\frac{\partial}{\partial x_i}(\bar{\rho}\tilde{T}\tilde{u}_i) = \tilde{\sigma}_{ij}\frac{\partial \tilde{u}_j}{\partial x_i} + \frac{\partial}{\partial x_i}\left(\tilde{k}\frac{\partial \tilde{T}}{\partial x_i}\right) - C_v\frac{\partial}{\partial x_i}(q_i) \tag{4}$$

where

$$\tilde{\sigma}_{ij} = -\bar{p}\delta_{ij} + \tilde{\mu}\left(\frac{\partial \tilde{u}_i}{\partial x_j} + \frac{\partial \tilde{u}_j}{\partial x_i} - \frac{2}{3}\frac{\partial \tilde{u}_k}{\partial x_k}\delta_{ij}\right) \tag{5}$$

represents the resolved-scale stress tensor. The effects of the small scales are present in these equations through the SGS stress tensor and the SGS heat flux,

$$\tau_{ij} = \bar{\rho}(\widetilde{u_i u_j} - \tilde{u}_i\tilde{u}_j) \tag{6}$$

$$q_i = \bar{\rho}(\widetilde{u_i T} - \tilde{u}_i\tilde{T}) \tag{7}$$

respectively, and require modeling. A tilde is used to denote Favre averages ($\tilde{f} = \overline{\rho f}/\bar{\rho}$). Also ρ is the density, T is the temperature, u_i is the velocity vector, and k is the thermal conductivity. The specific heats at constant volume C_v and at constant pressure C_p are assumed in this study to be constant. The large-scale molecular viscosity $\tilde{\mu}$ is assumed to obey the power law $\tilde{\mu}/\tilde{\mu}_0 = (\tilde{T}/\tilde{T}_0)^{0.76}$, whereas the large-scale pressure $\bar{p}$ is obtained from the filtered equation of state $\bar{p} = \bar{\rho}R\tilde{T}$. The molecular Prandtl number Pr is assumed to be 0.7. Note, that in deriving Eqs. (2–4), the viscous, pressure-dilatation and conduction terms were approximated in a similar fashion as by Erlebacher et al.[8]

B. Dynamic Modeling of the Subgrid Scales

The SGS terms [Eqs. (6) and (7)] are modeled here using a compressible flow version of the dynamic SGS model of Germano et al.[1]; for details, see Refs. 2 and 3. The model involves three coefficients, C, C_I, and Pr_t. They are automatically adjusted, as time progresses, based on the resolved flowfield information with the aid of a second filter (test filter $\hat{G}$) that has a filter width coarser than the grid used to perform the computations.

A refinement to the Moin et al.[2] model has been proposed by Lilly.[3] The two versions differ only on the type of a contraction used to determine uniquely the model coefficients, as is described later in this section. Both versions were tested in simulations, and comparative results are presented in Sec. III.B. The results presented in other sections were obtained using the Lilly contraction.

The model parameterization for the SGS stress and the SGS heat flux is given by

$$\tau_{ij} - \tfrac{1}{3}\tau_{kk}\delta_{ij} = -2C\bar{\rho}\Delta^2|\tilde{S}|\left(\tilde{S}_{ij} - \tfrac{1}{3}\tilde{S}_{kk}\delta_{ij}\right) \tag{8}$$

$$\tau_{kk} = 2C_I\bar{\rho}\Delta^2|\tilde{S}|^2 \tag{9}$$

$$q_i = -\frac{\bar{\rho}C\Delta^2|\tilde{S}|}{Pr_t}\frac{\partial \tilde{T}}{\partial x_i} \tag{10}$$

where

$$\tilde{S}_{ij} = \frac{1}{2}\left(\frac{\partial \tilde{u}_i}{\partial x_j} + \frac{\partial \tilde{u}_j}{\partial x_i}\right), \qquad |\tilde{S}| = (2\tilde{S}_{ij}\tilde{S}_{ij})^{\frac{1}{2}}$$

$$\Delta = (\Delta x\Delta y\Delta z)^{\frac{1}{3}}$$

The model coefficients are computed from

$$C = \left\langle\left(L_{ij} - \tfrac{1}{3}L_{kk}\delta_{ij}\right)A_{ij}\right\rangle / \langle M_{pq}A_{pq}\rangle \tag{11}$$

$$C_I = \langle L_{kk}\rangle / \langle 2\hat{\bar{\rho}}\,\hat{\Delta}^2|\hat{\tilde{S}}|^2 - 2\Delta^2\widehat{\bar{\rho}|\tilde{S}|^2}\rangle \tag{12}$$

$$Pr_t = C(\langle N_iB_i\rangle / \langle -K_jB_j\rangle) \tag{13}$$

where $\hat{}$ denotes test-filtered quantities, $\hat{\Delta} = (\hat{\Delta}_1\hat{\Delta}_2\hat{\Delta}_3)^{1/3}$ ($\hat{\Delta}_i$ is the width of the test filter in the ith direction), $\langle\,\rangle$ denotes some kind of averaging procedure, and

$$L_{ij} = \widehat{\bar{\rho}\tilde{u}_i\tilde{u}_j} - (1/\hat{\bar{\rho}})\widehat{\bar{\rho}\tilde{u}_i}\,\widehat{\bar{\rho}\tilde{u}_j} \tag{14}$$

$$M_{ij} = -2\hat{\Delta}^2\hat{\bar{\rho}}\,|\hat{\tilde{S}}|\left(\hat{\tilde{S}}_{ij} - \tfrac{1}{3}\hat{\tilde{S}}_{kk}\delta_{ij}\right) + 2\Delta^2\,\widehat{\bar{\rho}|\tilde{S}|\left(\tilde{S}_{ij} - \tfrac{1}{3}\tilde{S}_{kk}\delta_{ij}\right)} \tag{15}$$

$$N_i = \hat{\Delta}^2\hat{\bar{\rho}}\,|\hat{\tilde{S}}|\frac{\partial \hat{\tilde{T}}}{\partial x_i} - \Delta^2\,\widehat{\bar{\rho}|\tilde{S}|\frac{\partial \tilde{T}}{\partial x_i}} \tag{16}$$

$$K_i = \widehat{\bar{\rho}\tilde{u}_i\tilde{T}} - \left(1/\hat{\bar{\rho}}\right)\widehat{\bar{\rho}\tilde{u}_i}\,\widehat{\bar{\rho}\tilde{T}} \tag{17}$$

Finally, depending on the choice of contraction used,

$$A_{ij} = \begin{cases} \tilde{S}_{ij}: & \text{Moin's version} \\ M_{ij}: & \text{Lilly's version} \end{cases} \tag{18}$$

and

$$B_i = \begin{cases} \dfrac{\partial \tilde{T}}{\partial x_i}: & \text{Moin's version} \\ N_i: & \text{Lilly's version} \end{cases} \tag{19}$$

The model requires the above averaging procedure, an ad hoc solution,[1] to prevent numerical instabilities due to a simplification made in the derivation of the expressions for the model coefficients. For flows having a direction of homogeneity, spatial averaging is usually performed along that direction. For the case of homogeneous turbulence, this results in volume averaging and is the approach taken in this study. For this type of flow, the model coefficients vary only with time.

C. Computer Implementation

The numerical method for the direct and large eddy simulations employed a pseudo-spectral Fourier collocation scheme for spatial differencing and a third-order Runge–Kutta method for advancing in time.[9] The validity of the numerical implementation of the dynamic model was established by performing a priori tests similar to those by Moin et al.[2] and comparing with their reported data.

III. Results

A. Capturing of Compressibility Effects

The ability of the dynamic model to capture compressibility effects was examined by performing LES of decaying isotropic turbulence and comparing with the results obtained from DNS. A number of simulations were conducted at different initial levels of compressibility and Reynolds numbers. The cases listed in Table 1 were considered.

The level of compressibility of the initial fields was controlled by either varying the initial turbulent Mach number M_t (cases 1–3), or the fraction of the turbulent kinetic energy initially contained in the dilatational velocity field χ (cases 4–6). The effect of the turbulent Reynolds number Re_T on compressibility was examined in cases 7, 8, and 3 and also in cases 4, 2, and 9. [Here, $M_t = q/c$, $\chi = (q^d/q)^2$, and $Re_T = \rho q^4/(\epsilon\mu)$, where q is the rms magnitude of the fluctuation velocity, c is the mean speed of sound, q^d is the

Table 1 Case parameters

Case	M_t	χ	Re_T
1	0.2	0	2742
2	0.4	0	2742
3	0.6	0	2742
4	0.4	0	2157
5	0.4	0.1	2157
6	0.4	0.2	2157
7	0.6	0	735
8	0.6	0	2156
9	0.4	0	6170

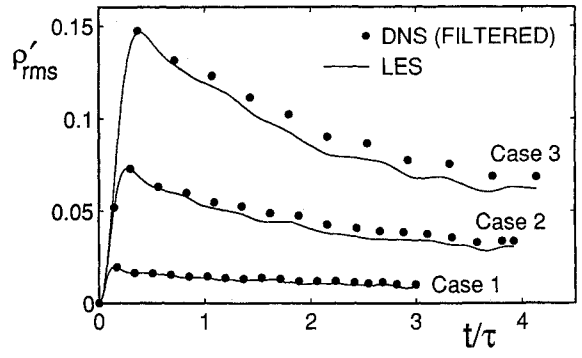

Fig. 1 Time evolutions of rms density fluctuations for cases 1–3; effects of initial M_t.

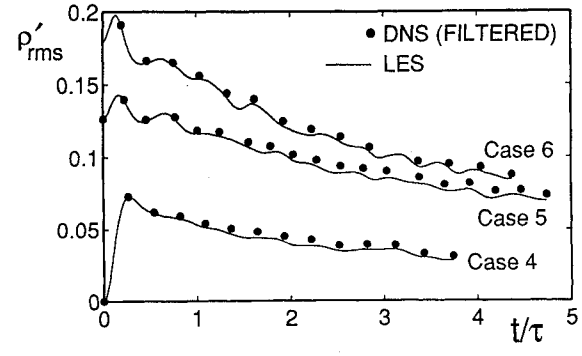

Fig. 2 Time evolutions of rms density fluctuations for cases 4–6; effects of initial χ.

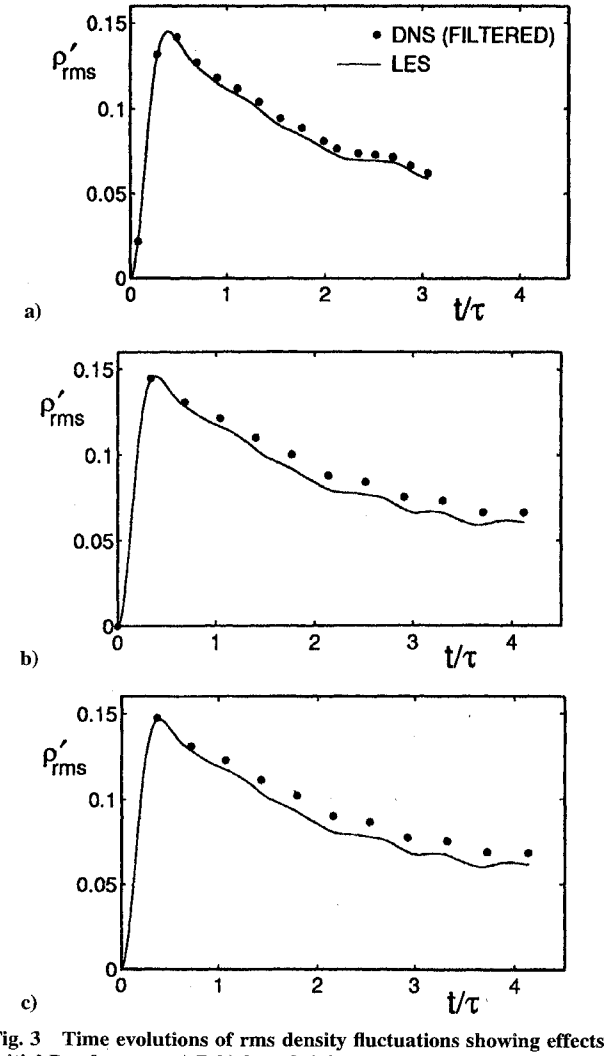

Fig. 3 Time evolutions of rms density fluctuations showing effects of initial Re_T for cases a) 7, b) 8, and c) 3.

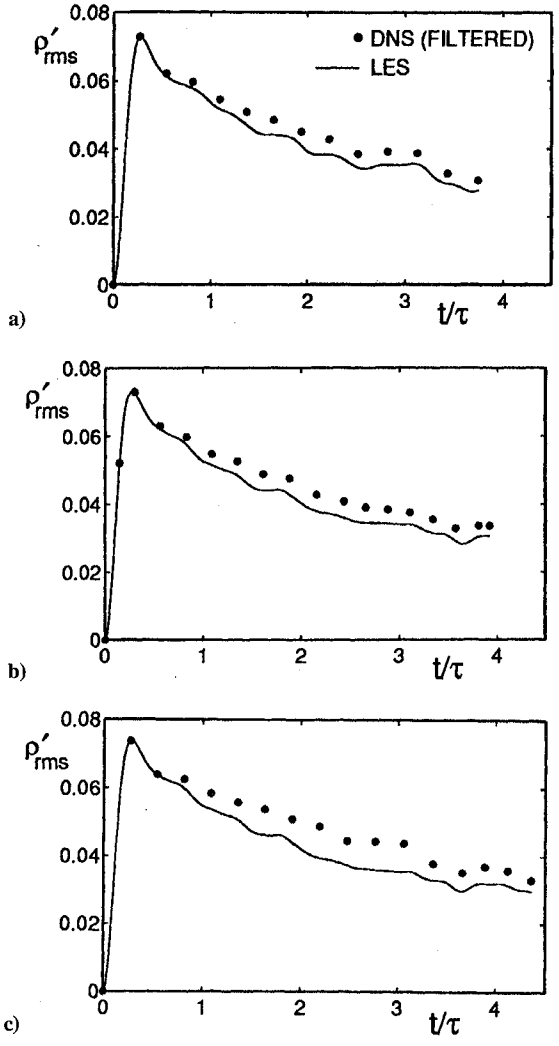

Fig. 4 Time evolutions of rms density fluctuations showing effects of initial Re_T for cases a) 4, b) 2, and c) 9.

rms magnitude of the dilatational fluctuation velocity, and ϵ is the dissipation rate of turbulent kinetic energy per unit mass.]

All cases with purely solenoidal initial velocity fields ($\chi = 0$) had uniform initial density and temperature fields, whereas the density and temperature fluctuations in the others were obtained from the isentropic relations and the condition for acoustic equilibrium (see Sarkar et al.[10]). The initial three-dimensional energy spectrum for each case was of the form

$$E(k) \propto k^4 \exp\left[-2(k/k_p)^2\right] \tag{20}$$

where the wave number of the peak of the spectrum k_p was set at 4. The LES were computed on $(32)^3$ grids, whereas the DNS were computed on $(128)^3$ grids.

Good, and percentwise consistent, agreement in all statistics considered was found between the LES and the DNS for all cases. This is shown, for example, in Figs. 1–4, where the evolutions of the rms density fluctuations between the LES and the (filtered) DNS data for the above sets of cases are compared. (The time axes in these figures have been scaled with the initial eddy turnover time τ, defined as the ratio of the lateral Taylor microscale and the rms fluctuation velocity in a direction.) Similar findings were obtained by comparing other statistical quantities, as well as one- and three-dimensional spectra, indicating that the dynamic SGS model seems to be capturing compressibility effects well for isotropic turbulence.

B. Comparison of Two Model Versions

In the preceding results, Lilly's version[3] of the dynamic model was employed. The Moin et al.[2] version was also tested for all cases. It predicted higher values for coefficient C, smaller values for coefficient C_I, and similar values with Lilly's version for Pr_t,

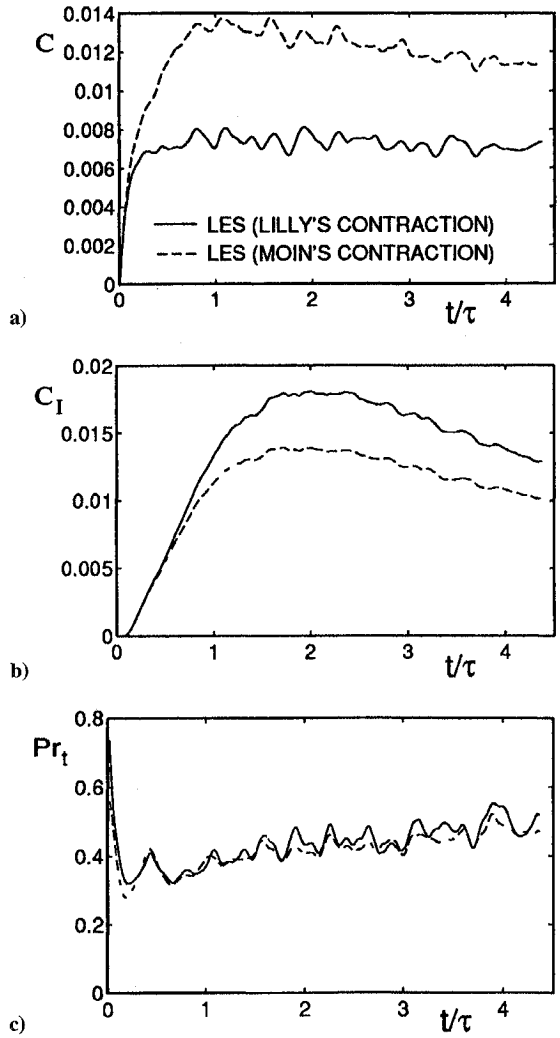

Fig. 5 Time evolutions of model coefficients showing effects of different contractions for case 6: a) C, b) C_I, and c) Pr_t.

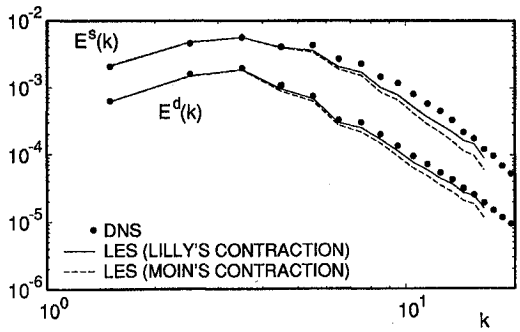

Fig. 6 Three-dimensional solenoidal and dilatational energy spectra for case 6 at $t/\tau = 4.37$; effects of different contractions.

as is shown, for case 6, in Fig. 5. Overall, the Moin et al. model also performed well but provided higher amounts of dissipation than Lilly's, as can be seen in the three-dimensional solenoidal and dilatational energy spectra for the same case shown in Fig. 6. This is most evident at higher wave numbers. The results are taken at a time when the turbulent kinetic energy had decayed to one-fourth of its initial value.

It should be noted that the values of Pr_t obtained from either version of the dynamic model were about 0.4–0.6 when the initial temperature field had a three-dimensional spectrum similar to the velocity's. In contrast, when the temperature was initially set to be uniform, Pr_t values higher than unity were predicted by the model. This behavior is believed to be due to differences in the initial transients of the temperature fields and is another indication for the need for dynamic modeling.

C. Effects of Varying the Test Filter Width

The only adjustable parameter in the dynamic model is the ratio $\alpha = \hat{\Delta}/\Delta$ of the widths of the test and the grid filter (see Sec. II.B). Based on a priori and a posteriori tests of incompressible transitional and turbulent channel flow, Germano et al.[1] suggested a value of 2 for future use. They also suggested further investigations using different types of flows. This value has since been adopted by other researchers and was used in most of the simulations presented here.

The sensitivity of the results on the choice of the filter width ratio was also examined here for two cases of highly compressible isotropic decaying turbulence (cases 6 and 9 from Table 1). Five values of α were considered: 1.6, 16/9, 2, 16/7, and 8/3. These correspond to Fourier cutoff wave numbers for the test filter of 10, 9, 8, 7, and 6, respectively. Note that the use of smaller or greater α values is undesirable, since it results in test-filtered quantities that are either almost unaffected by the filtering or contain only very large-scale information, respectively, and usually leads to ill-predicted model coefficients. Results for such cases are not presented here.

Noticeable differences in the evolutions of the model coefficients were found when different values for α were used in the simulations, as is shown for case 6 in Fig. 7. (The model coefficients were also calculated a priori from DNS results, and similar differences were seen.)

Surprisingly enough, the choice of α seems to have only a very small effect on the LES results.[1] For instance, the rms density fluctuations for case 6 (shown in Fig. 2 for $\alpha = 2$) varied by less than 3% for the five values of α considered (the differences are graphically indistinguishable). This difference was even smaller for case 9. Best agreement with the DNS was obtained when this parameter was set to 2.

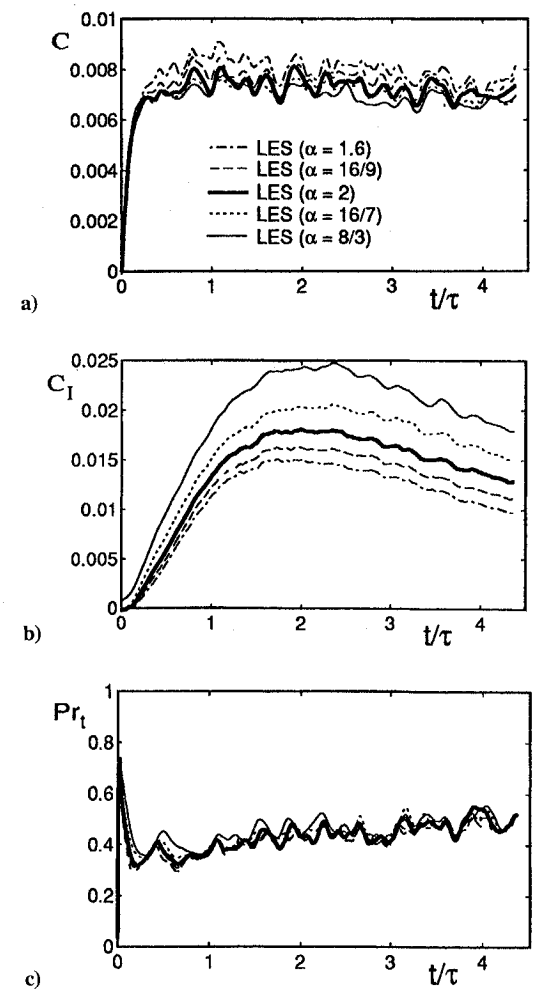

Fig. 7 Time evolutions of model coefficients showing effects of filter width ratio for case 6: a) C, b) C_I, and c) Pr_t.

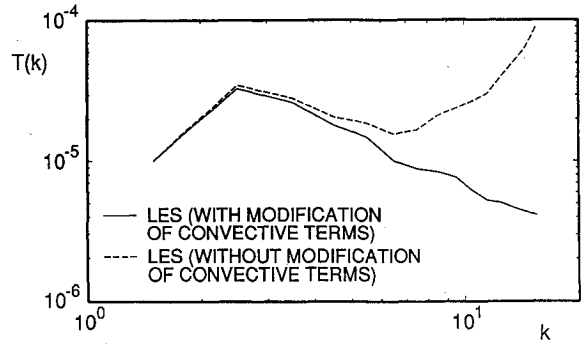

Fig. 8 Three-dimensional temperature spectra from simulations of the Comte-Bellot and Corrsin experiment; effects of modifying the convective terms.

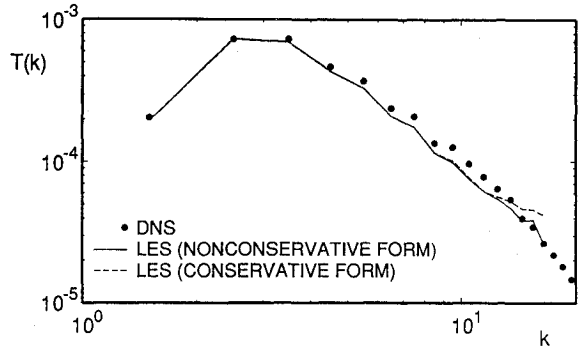

Fig. 9 Three-dimensional temperature spectra for case 6 at $t/\tau = 2.23$; effects of reformulating the energy equation.

D. Modification of the Convective Terms

It should be noted that the convective terms in the filtered momentum and filtered energy equations, Eqs. (3) and (4), were modified to the skew-symmetric form,

$$\frac{\partial}{\partial x_j}(f\tilde{u}_j) \rightarrow \frac{1}{2}\frac{\partial}{\partial x_j}(f\tilde{u}_j) + \frac{1}{2}\tilde{u}_j\frac{\partial f}{\partial x_j} + \frac{1}{2}f\frac{\partial \tilde{u}_j}{\partial x_j} \tag{21}$$

where f refers to $\bar{\rho}\tilde{u}_i$ and $\bar{\rho}\tilde{T}$, respectively.

This modification reduces the effect of aliasing errors,[11,12] which seems to be a bigger problem in LES than in DNS because the flowfields are less well resolved. Shown in Fig. 8 are three-dimensional temperature spectra from LES of the (high Reynolds number) Comte-Bellot and Corrsin experiment[13] (see Sec. III.F.2 for a description of the simulation). The LES without modifying the convective terms had a pile-up at high wave numbers, which led to instabilities, whereas the simulation with the modified terms was well behaved.

E. Alternative Formulation for the Energy Equation

In LES, there is also a choice in the formulation of the energy equation. The most popular approach is the solution of a nonconservative formulation (internal energy equation), since it requires only modeling of the SGS heat flux (see Sec. II.A). In contrast, if a conservative form (total energy equation) is used instead, then modeling of additional SGS terms is required. An alternative procedure, which does not require any additional modeling, is to solve for the pseudo total energy, defined as

$$\bar{\phi} = \bar{\rho}C_v\tilde{T} + \bar{\rho}\tilde{u}_i\tilde{u}_i/2 \tag{22}$$

The resulting equation is

$$\frac{\partial}{\partial t}(\bar{\phi}) + \frac{\partial}{\partial x_i}(\bar{\phi}\tilde{u}_i) = \frac{\partial}{\partial x_i}(\tilde{\sigma}_{ij}\tilde{u}_j) - \tilde{u}_j\frac{\partial}{\partial x_i}(\tau_{ij}) + \frac{\partial}{\partial x_i}\left(\tilde{k}\frac{\partial \tilde{T}}{\partial x_i}\right) - C_v\frac{\partial}{\partial x_i}(q_i) \tag{23}$$

This form is not in strong conservation law form; however, we refer to it here as the conservative form.

In LES of decaying compressible turbulence (case 6 from Table 1) both formulations performed well, but the nonconservative form was more accurate. The conservative form was found to have somewhat of a pileup in the high wave number part of the density and temperature spectra, as is shown in Fig. 9. This is believed to be due to aliasing errors originating from evaluating the temperature from the pseudo total energy.

F. Effects of Employing Different Spatial Test Filters

As was discussed in Sec. II.B, the dynamic model requires (test) filtering the resolved large-scale field. In flows that are homogeneous in at least two directions, the filtering can be performed efficiently (and exactly) in wave space using fast Fourier transforms. In more complex inhomogeneous flows, this is not possible, and some kind of discrete filtering has to be applied in physical space. In the next two sections, the formulation and testing of such filters is presented.

1. *Formulation of Spatial Filters*

Many different formulations of spatial filters were examined to determine their behavior in Fourier space. This was done because we believe it would be desirable for the spatial filter to have properties similar to the sharp cutoff filter.

For uniformly spaced grids, the spatial filters are formulated as follows:

$$\hat{f}_j + \sum_{n=1}^{N_i}\alpha_n\frac{\hat{f}_{j-n} + \hat{f}_{j+n}}{2} = \sum_{n=0}^{N_e-1}a_n\frac{f_{j-n} + f_{j+n}}{2} \tag{24}$$

where f_j is the function value at node j and $\hat{f}_j$ is the corresponding filtered function value. N_i is the number of implicit coefficients, which are given by $\{\alpha_n\}$, and N_e is the number of explicit coefficients, which are $\{a_n\}$.

The Fourier transform of the filtered function is given by $\hat{\mathcal{F}} = \mathcal{G}\mathcal{F}$, where $\mathcal{F}$ is the Fourier transform of the function and $\mathcal{G}$ is the filter transfer function. For the filter formulation (24), the filter transfer function is

$$\mathcal{G}_k = \left[\sum_{n=0}^{N_e-1}a_n\cos\left(\frac{2\pi kn}{N}\right)\right]\Bigg/\left[1 + \sum_{m=1}^{N_i}\alpha_m\cos\left(\frac{2\pi km}{N}\right)\right] \tag{25}$$

where k is the wavenumber and N is the number of grid points.

The first filters to be considered are approximations to the top-hat filter in physical space. The top-hat filter is defined by

$$\hat{G}(x - x') = \begin{cases} 1 & \text{if } x - \hat{\Delta}/2 \le x' \le x + \hat{\Delta}/2 \\ 0 & \text{otherwise} \end{cases} \tag{26}$$

where the filter width $\hat{\Delta}$ is assumed here equal to $2\Delta x$ (as was suggested in Sec. III.C). The convolution integral in Eq. (1) can be approximated in various ways. Using three collocation points and the trapezoid rule gives $a_0 = 1/2$ and $a_1 = 1/2$. With three collocation points one can improve the accuracy of the integration by using Simpson's rule, which gives $a_0 = 2/3$ and $a_1 = 1/3$. If the integration is done analytically, then a spectrally accurate formula is obtained.

The filter transfer functions for these schemes are shown in Fig. 10a against that of the sharp cutoff filter. The top-hat filter behaves very differently from the sharp cutoff filter and is more like the Gaussian filter in that some of the low wave number modes are reduced in amplitude whereas some of the high wave number modes are retained.

A second set of filters is obtained by approximating the sharp cutoff filter in a least squares sense, with certain constraints imposed. Three constraints are considered. Constraint 1 is that the filter be mean preservering. This is important because the filter is supposed to separate large and small scales and should not alter a uniform field. For the filter to be mean preserving, it is necessary that $\mathcal{G}(0) = 1$. Constraint 2 is that the end point of the filter transfer function is fixed to be zero; i.e., $\mathcal{G}(k = N/2) = 0$. This constraint is not required on any physical basis; however, we believe it is a desirable property of the filter transfer function. Constraint 3 is that the ratio of the

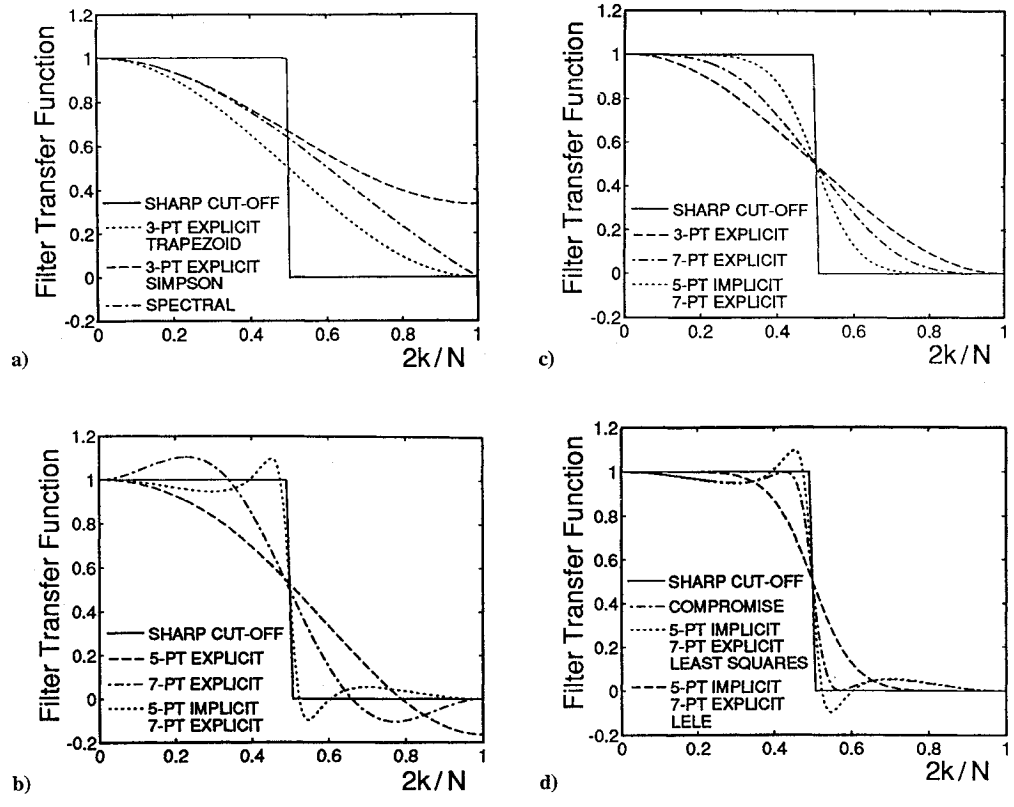

Fig. 10 Comparison of filter transfer functions for various spatial filters: a) top-hat filters, b) sharp cutoff least squares filters, c) Lele filters, and d) compromise filter.

filter width to the grid spacing, $\hat{\Delta}/\Delta x$, be 2, since this is the chosen standard value.

To implement constraint 3, one has to define the filter width for a given filter. We have chosen to define the filter width in a manner analogous to how the integral length scale is defined for a two-point correlation. For a discrete filter this corresponds to

$$\hat{\Delta} = \sum_{j=1}^{N} \frac{\hat{G}_j}{\hat{G}_1} \Delta x \tag{27}$$

Since the filters are mean preserving

$$\sum_{j=1}^{N} \hat{G}_j = \mathcal{G}_0 = 1 \tag{28}$$

and

$$\frac{\hat{\Delta}}{\Delta x} = \frac{1}{\hat{G}_1} = 1 \Big/ \frac{1}{N} \sum_{k=-N/2+1}^{N/2} \mathcal{G}_k \tag{29}$$

This definition is dependent on the number of grid points N, which is undesirable. A more useful formulation can be obtained by letting $k' = 2k/N$, $\Delta k' = 2\Delta k/N$ (where $\Delta k = 1$) and $\mathcal{G}'(k') = \mathcal{G}(k)$, where $\mathcal{G}(k)$ is given by Eq. (25), so that

$$\frac{\hat{\Delta}}{\Delta x} = 1 \Big/ \frac{1}{2} \sum_{k=-N/2+1}^{N/2} \mathcal{G}'(k')\, \Delta k' \tag{30}$$

Taking the limit $N \to \infty$ and using the symmetry of $\mathcal{G}'$ results in

$$\frac{\hat{\Delta}}{\Delta x} = 1 \Big/ \int_0^1 \mathcal{G}'(k')\, dk' \tag{31}$$

This definition is consistent with the length scale obtained from the cutoff wave number when a sharp cutoff filter is used, which is the reason it was chosen. An alternate definition in terms of the second moment of the filter function was used by Leonard[14] for the top-hat filter and the Gaussian filter; however, for the sharp cutoff filter such a definition gives an infinite filter width, and for some of the other filters considered in this study, an imaginary filter width is obtained. Therefore, the definition given in Eq. (31) was adopted.

The least squares problem is formulated as minimizing the integrated square difference between the filter transfer function $\mathcal{G}'(k')$ and the transfer function for the sharp cutoff filter $\mathcal{G}'_{sco}(k')$. The free parameters are the filter coefficients $\{a_n\}$ and $\{\alpha_m\}$. From constraint 1 we have

$$\mathcal{G}'(0) = \left[\sum_{n=0}^{N_e-1} a_n \Big/ \left(1 + \sum_{m=1}^{N_i} \alpha_m \right) \right] = 1 \tag{32}$$

Constraint 2 gives

$$\mathcal{G}'(k' = 1) = 0 = \sum_{n=0}^{N_e-1} a_n \tag{33}$$

These two equations can be solved for a_{N_e-1} and a_{N_e-2} in terms of the other parameters, so that the numbers of degrees of freedom is reduced by two. Constraint 3 was enforced by using a penalty function. The function to be minimized is

$$E = \int_0^1 [\mathcal{G}'(k') - \mathcal{G}'_{sco}(k')]^2\, dk' + A\left(\frac{\hat{\Delta}}{\Delta x} - 2 \right)^2 \tag{34}$$

The Nelder–Mead simplex search algorithm[15] was implemented to solve the minimization problem. The integrals needed to evaluate E were calculated using Romberg integration with the error tolerance set to 10^{-14}. The constant A was set to 10^{10} so that constraint 3 was met with an error on the order of 10^{-6}. For explicit filters, the integrals can be evaluated analytically, and the minimization problem can be solved exactly. This was used as a check of the numerical procedure. For this case, Eq. (31) reduces to

$$\hat{\Delta}/\Delta x = 1/a_0 \tag{35}$$

Table 2 Summary of spatial filters tested in simulations

Filter	a_0	a_1	a_2	a_3	α_1	α_2
1 3-pt explicit, trapezoid	0.5	0.5				
2 3-pt explicit, Simpson	0.6666667	0.3333333				
3 5-pt explicit, least squares	0.4726761	0.5819719	−0.05464480			
4 7-pt explicit, least squares	0.5	0.6744132	0	−0.1744132		
5 5-pt implicit–7-pt explicit, least squares	0.5	0.8105146	0.4830535	0.1725389	0	0.9661071
6 5-pt implicit–7-pt explicit, Lele	0.5	0.75	0.3	0.05	0	0.6
7 5-pt implicit–7-pt explicit, compromise	0.5	0.8056734	0.4684092	0.1627358	0	0.9368185

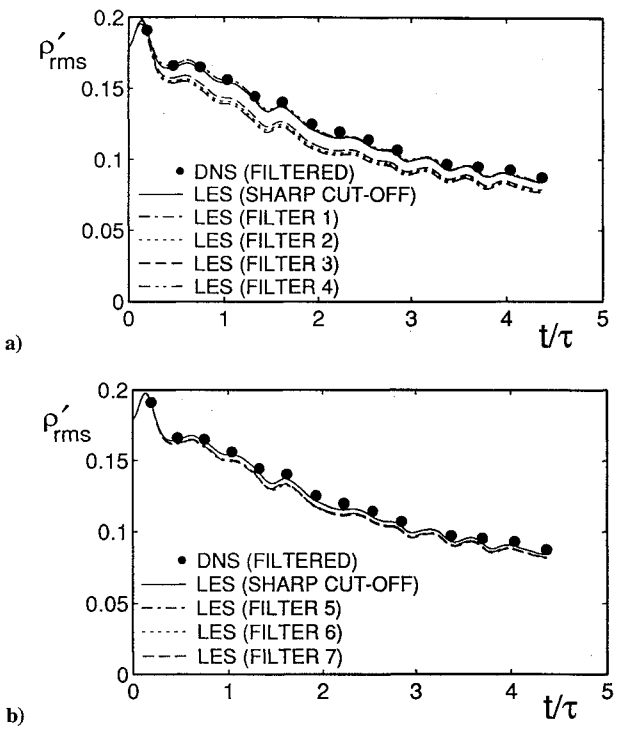

Fig. 11 Time evolutions of rms density fluctuations for case 6; effects of spatial filters: a) explicit and b) implicit.

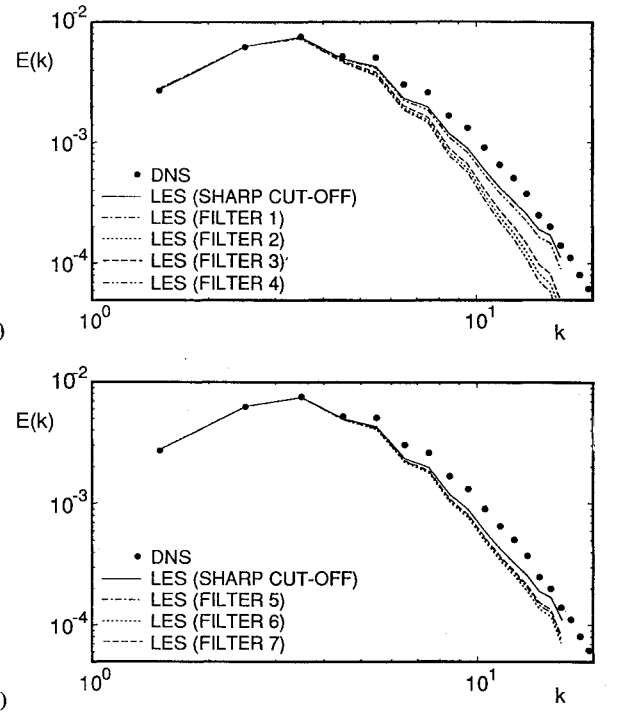

Fig. 12 Three-dimensional energy spectra for case 6 at $t/\tau = 4.37$; effects of spatial filters: a) explicit and b) implicit.

The resulting filter coefficients are given in Table 2. The three-point explicit filter is the same as the trapezoid filter. No five-point explicit filter was found that met all of the constraints, and so constraints 2 and 3 were dropped for the five-point explicit filter shown. The highest order explicit filter considered is a seven-point filter. A number of implicit filters were found. The one discussed here is a five-point implicit–seven-point explicit filter.

The least squares filters are compared to the sharp cutoff filter in Fig. 10b. As the number of filter coefficients is increased, better agreement with the sharp cutoff filter is obtained, as expected. However, the filter transfer functions are oscillatory and display large amplitude overshoots, which is believed to be undesirable.

A third set of filters is obtained following Lele[16] in which a different set of constraints are placed on the filter transfer function. To compare these filters to the sharp cutoff filter with $\hat{\Delta}/\Delta x = 2$, the extra constraint $\mathcal{G}(k = N/4) = 1/2$ was imposed. The filters obtained are shown in Fig. 10c. In general, the filters are smooth, monotonically decreasing from 1 to 0. However, the filters are not as sharp as the five-point implicit method obtained from the least squares approach. Note that the three-point explicit filter is the same as the trapezoid filter.

The filters obtained from Lele's formulation are very smooth, whereas the filters found from the least squares approach are much sharper but exhibit oscillations. In an attempt to reach a compromise between the two filters, we constructed filters obtained by combining the filter coefficients in the following way:

$$a_n = \psi a_n^{\text{ls}} + (1-\psi)a_n^{\text{Lele}}, \qquad \alpha_n = \psi \alpha_n^{\text{ls}} + (1-\psi)\alpha_n^{\text{Lele}} \quad (36)$$

Figure 10d shows the transfer function for the five-point implicit–seven-point explicit filter with $\psi = 0.92$. This compromise filter gives a transfer function that is sharper than that from the Lele formulation but does not have as large an overshoot as that from the least squares approach.

2. *Testing of Spatial Filters*

A number of spatial filters from the preceding section were tested in simulations. The filters considered are shown in Table 2 (see also Fig. 10). Homogeneous flow test cases were chosen, so that the effects of these filters can be compared to that of the sharp cutoff filter, defined in wave space, as well as against available DNS or experimental data.

Results from simulations of a highly compressible decaying isotropic flow (case 6 from Table 1) are presented first. The histories of the rms density fluctuations are compared in Fig. 11. Figure 12 shows comparisons of three-dimensional energy spectra taken at a time when the turbulent kinetic energy had decayed to one-fourth of its initial value. The results from a DNS are also included in these figures for further comparison. The evolutions of the model coefficient C are shown in Fig. 13. All spatial filters are found to be more dissipative at higher modes than the sharp cutoff. All implicit filters performed well and, among them, filter 7 was found to be the best candidate. Most of the explicit filters were very dissipative and performed poorly, with the exception of filter 4 which gave results very similar to those from the sharp cutoff filter. However, this filter predicted small negative values for the coefficient C_I and, consequently, from Eq. (9), negative values for the subgrid-scale turbulent kinetic energy τ_{ii}. This may, in some cases, lead to numerical instabilities, although it did not here.

The spatial filters were also tested for the case of a nearly incompressible turbulence. The isotropic grid-generated (high Reynolds

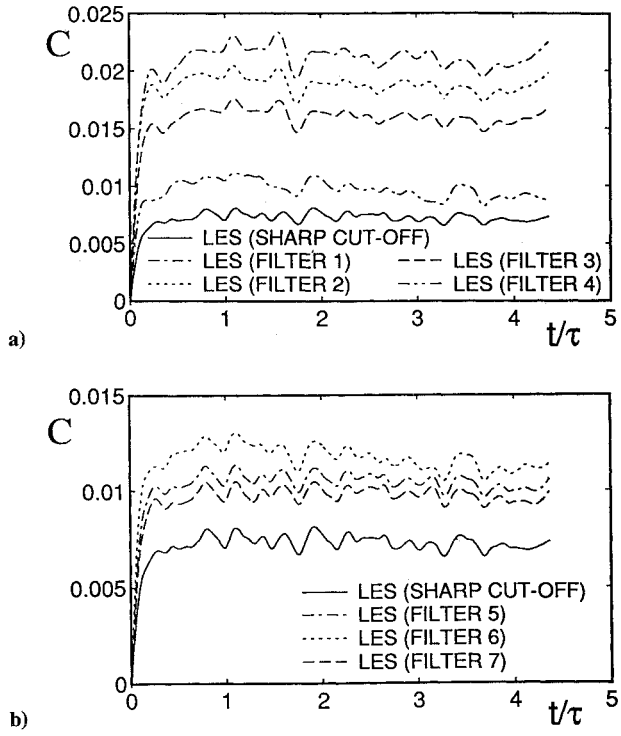

Fig. 13 Time evolution of model coefficient C for case 6; effects of spatial filters: a) explicit and b) implicit.

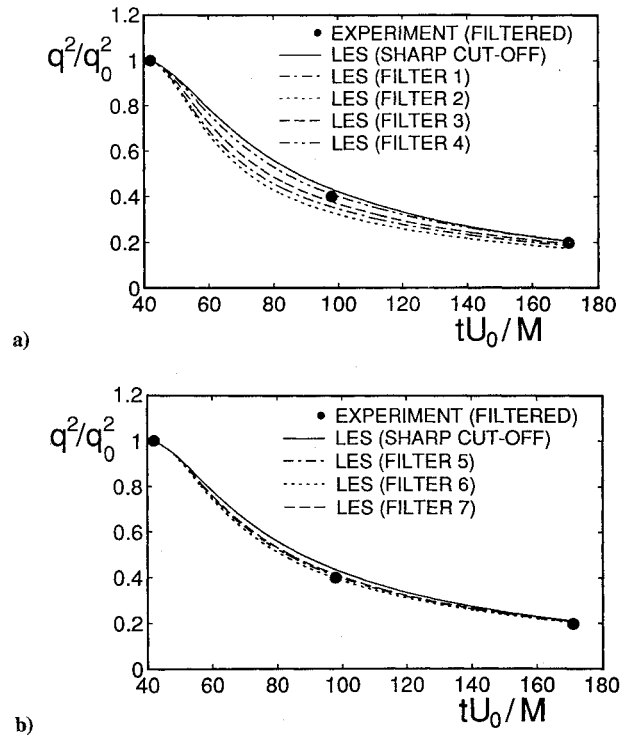

Fig. 14 Time evolution of turbulent kinetic energy from simulations of Comte-Bellot and Corrsin's experiment; effects of spatial filters: a) explicit and b) implicit.

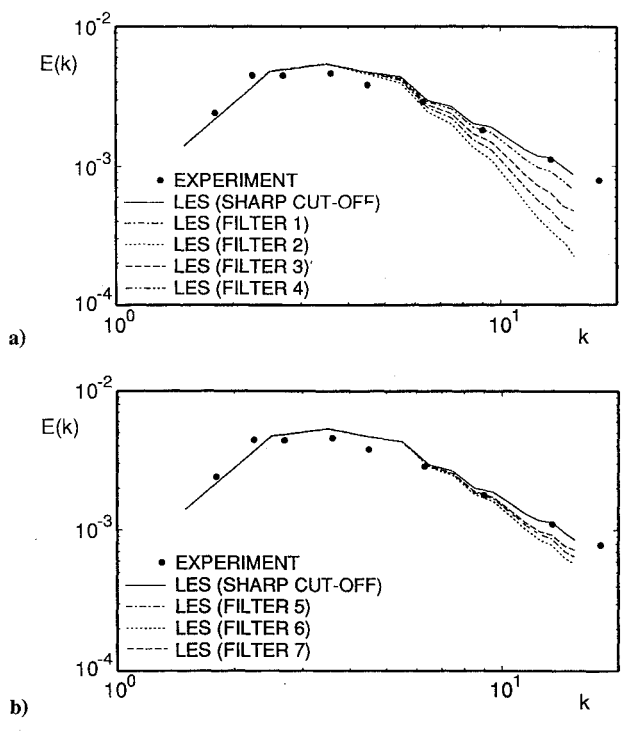

Fig. 15 Three-dimensional energy spectra from simulations of Comte-Bellot and Corrsin's experiment at $tU_0/M = 98$; effects of spatial filters: a) explicit and b) implicit.

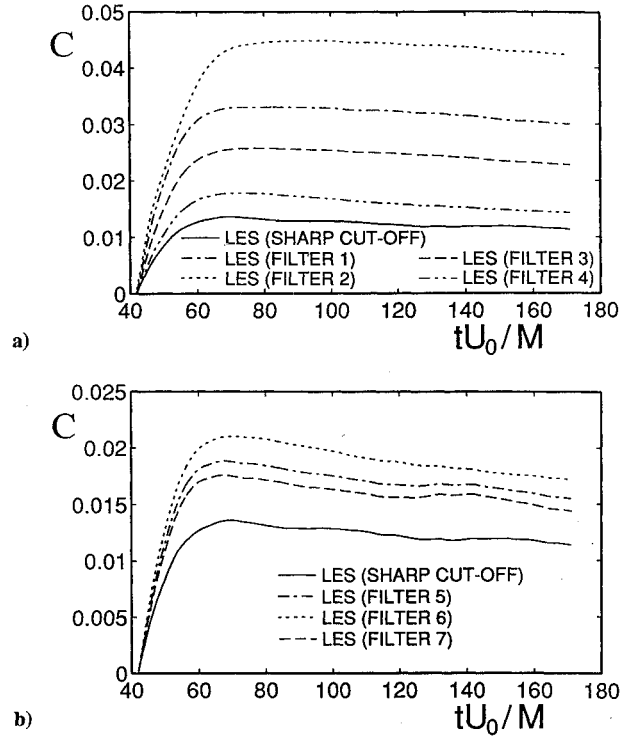

Fig. 16 Time evolution of model coefficient C from simulations of Comte-Bellot and Corrsin's experiment; effects of spatial filters: a) explicit and b) implicit.

number) turbulence experiment of Comte-Bellot and Corrsin[13] was simulated as a temporal decay on a $(32)^3$ grid. The initial velocity fields for the simulations were purely solenoidal and designed to have the same three-dimensional spectrum as that reported at $tU_0/M = 42$ in the experiment (where U_0 is the mean flow velocity and M is the grid size). The initial pressure fields were computed from the incompressible Poisson equation, while the density was assumed to be uniform. The initial Mach number was set to 0.3.

The sharp cutoff filter was employed first in the dynamic model. The predicted time development of the turbulent kinetic energy and the three-dimensional energy spectra compare well with the available experimental data, as shown in Figs. 14 and 15, respectively.

The performance of the spatial filters was then examined. Figures 14 and 15 also present results from these simulations. The evolution of the model coefficient C predicted from the various spatial filters are compared against the one from the sharp cutoff filter in Fig. 16. Filter 6 was found to be the most dissipative of the implicit

filters. However, all of these filters performed well and similarly to the sharp cutoff filter. Filter 4, the seven-point explicit filter, again performed very well, in contrast to the three-point and five-point explicit filters, which provided great amounts of dissipation.

For the Comte-Bellot and Corrsin simulation, we neglected C_I on the basis that for nearly-incompressible flows τ_{kk} is small compared to the thermodynamic pressure.[8,17,18] This was done to avoid instabilities in the computations that occurred during the initial transient period for some of the spatial filters. However, negligible difference on the results was observed when the sharp cutoff filter was used and C_I was computed from the dynamic model.

IV. Conclusions

Several issues involving the use of the dynamic SGS model in performing LES of compressible turbulent flows have been examined by employing the model in simulations and comparing with results from DNS or experiments. Decaying isotropic turbulence was considered in order to evaluate the performance of the model separately from the effects of inhomogeneity.

We conducted a parametric study where the levels of compressibility of the initial flow fields were varied. The model, with its ability to adjust itself to the flow conditions, was found to predict well, from a statistical viewpoint, the bulk of the flow. The dynamic model was able to capture compressibility effects well and does not require any explicit compressibility corrections.

In performing LES of inhomogeneous compressible turbulent flows using the dynamic model, the filtering operation required by the model can not be done in wave space but, rather, has to be approximated in physical space. We have examined the behavior of several implicit and explicit spatial filters in wave space. We also conducted simulations of highly compressible and high Reynolds number nearly incompressible cases of decaying isotropic turbulence to study the performance of such filters against that of the sharp cutoff filter defined conveniently in Fourier space. The five-point implicit–seven-point explicit filters examined performed extremely well and should be considered as good candidates for future use. However these filters would be more expensive to employ than explicit ones. The former filters have transfer functions that are much sharper than the other filters near the cutoff mode, but exhibit oscillations that as suggested by the simulations are not of serious concern. The seven-point explicit filter gave good results also; however, it predicted small negative values for model coefficient C_I, which is undesirable. The three-point and five-point explicit filters were very dissipative, especially in the high Reynolds number simulation.

Two versions of the dynamic model were employed and tested in LES. The version by Lilly[3] was found to be more accurate than the version by Moin et al.[2]

A number of simulations were also performed to study the effect of the filter width ratio—the only adjustable parameter in the dynamic model. The results suggest a great insensitivity of the model to this parameter. Best agreement with the results from DNS was obtained when this parameter was set to 2.

Modification of the convective terms in the filtered momentum and filtered energy equations improves the accuracy of the simulations, as well as the stability of the numerical method. In addition, the nonconservative formulation of the energy equation was found to be somewhat better than the conservative form.

Acknowledgments

This work was supported by NASA Langley under Grant NAG-1-1509. Computer resources were provided by the National Academy of Sciences and Purdue University. The authors would like to thank Thomas Lund and Ugo Piomelli for their helpful suggestions concerning this work.

References

[1]Germano, M., Piomelli, U., Moin, P., and Cabot, W., "A Dynamic Subgrid-scale Eddy-viscosity Model," *Physics of Fluids A*, Vol. 3, July 1991, pp. 1760–1765.

[2]Moin, P., Squires, K., Cabot, W., and Lee, S., "A Dynamic Subgrid-scale Model for Compressible Turbulence and Scalar Transport," *Physics of Fluids A*, Vol. 3, Nov. 1991, pp. 2746–2757.

[3]Lilly, D. K., "A Proposed Modification of the Germano Subgrid-scale Closure Method," *Physics of Fluids A*, Vol. 4, March 1992, pp. 633–635.

[4]Wong, V. C., "A Proposed Statistical-dynamic Closure Method for the Linear or Nonlinear Subgrid-scale Stresses," *Physics of Fluids A*, Vol. 5, May 1992, pp. 1080–1082.

[5]Ghosal, S., Lund, T. S., and Moin, P., "A Local Dynamic Model for Large Eddy Simulation," *Annual Research Briefs-1992*, Center for Turbulence Research, Stanford Univ., Stanford, CA, 1992, pp. 3–25.

[6]Piomelli, U., and Liu, J., "Large Eddy Simulation of Rotating Channel Flows Using a Localized Dynamic Model," *74th AGARD/FDP Symposium on Application of Direct and Large Eddy Simulation to Transition and Turbulence*, AGARD-CP-551, 3.1–3.9, Chania, Greece, 1994.

[7]El Hady, N. M., Zang, T. A., and Piomelli, U., "Applications of the Dynamic Subgrid-scale Model to Axisymmetric Transitional Boundary Layer at High Speed," *Physics of Fluids A*, Vol. 6, March 1994, pp. 1299–1309.

[8]Erlebacher, G., Hussaini, M. Y., Speziale, C. G., and Zang, T. A., "Toward the Large-eddy Simulation of Compressible Turbulent Flows," *Journal of Fluid Mechanics*, Vol. 238, May 1992, pp. 155–185.

[9]Blaisdell, G. A., Mansour, N. N., and Reynolds, W. C., "Compressibility Effects on the Growth and Structure of Homogeneous Turbulent Shear Flow," *Journal of Fluid Mechanics*, Vol. 256, Nov. 1993, pp. 443–485.

[10]Sarkar, S., Erlebacher, G., Hussaini, M. Y., and Kreiss, H. O., "The Analysis and Modeling of Dilatational Terms in Compressible Turbulence," *Journal of Fluid Mechanics*, Vol. 227, June 1991, pp. 473–493.

[11]Zang, T. A., "On the Rotational and Skew-symmetric Forms for Incompressible Flow Simulations," *Applied Numerical Mathematics*, Vol. 7, Jan. 1991, pp. 27–40.

[12]Blaisdell, G. A., Spyropoulos, E. T., and Qin, J. H., "The Effect of the Formulation of Nonlinear Terms on Aliasing Errors in Spectral Methods," *Applied Numerical Mathematics* (submitted for publication).

[13]Comte-Bellot, G., and Corrsin, S., "Simple Eulerian Time Correlation of Full and Narrow Band Velocity Signals in Grid Generated, Isotropic Turbulence," *Journal of Fluid Mechanics*, Vol. 48, July 1971, pp. 273–337.

[14]Leonard, A., "On the Energy Cascade in Large-eddy Simulations of Turbulent Fluid Flows," *Advances in Geophysics*, Vol. 18A, 1974, pp. 237–248.

[15]Press, W. H., Flannery, B. P., Teukolsky, S. A., and Vetterling, W. T., *Numerical Recipes: The Art of Scientific Computing*, Cambridge Univ. Press, Cambridge, England, UK, 1986, p. 289.

[16]Lele, S. K., "Compact Finite Difference Schemes with Spectral-like Resolution," *Journal of Computational Physics*, Vol. 103, Nov. 1992, pp. 16–42.

[17]Zang, T. A., Dahlburg, R. B., and Dahlburg, J. P., "Direct and Large Eddy Simulations of Three-Dimensional Compressible Navier–Stokes Turbulence," *Physics of Fluids A*, Vol. 4, Jan. 1992, pp. 127–140.

[18]Sreedhar, M., and Ragab, S., "Large Eddy Simulation of Longitudinal Stationary Vortices," *Physics of Fluids A*, Vol. 6, July 1994, pp. 2501–2514.